THE ASTROPHYSICAL JOURNAL, 496:L75–L78, 1998 April 1

JET-DRIVEN MOTIONS IN THE NARROW-LINE REGION OF NGC 1068[1]

D. J. AXON[2,3] AND A. MARCONI[4,5]
Space Telescope Science Institute, 3700 San Martin Drive, Baltimore, MD 21218
A. CAPETTI
Osservatorio Astronomico di Torino, 10025 Pino Torinese, Italy
F. D. MACCHETTO[2] AND E. SCHREIER
Space Telescope Science Institute, 3700 San Martin Drive, Baltimore, MD 21218
AND
A. ROBINSON
Division of Physics and Astronomy, Department of Physical Sciences, University of Hertfordshire, College Lane, Hatfield, Hertfordshire, AL10 9AB, England, UK
Received 1997 August 4; accepted 1998 January 9; published 1998 March 11

ABSTRACT

We have obtained *Hubble Space Telescope* Faint Object Camera (FOC) f/48 long-slit spectroscopy of the inner 4″ of the narrow-line region (NLR) of NGC 1068 between 3500 and 5400 Å with a spectral resolution of 1.78 Å pixel^{-1}. At a spatial scale of 0.″0287 pixel^{-1} these data provide an order-of-magnitude improvement in resolution over previous ground-based spectra and allow us to trace the interaction between the radio jet and the gas in the NLR. Our results show that within $\pm 0.''5$ of the radio jet the emission lines are kinematically disturbed and split into two components whose velocity separation is 1500 km s^{-1}. The filaments associated with the radio lobe also show a redshifted kinematic disturbance on the order of 300 km s^{-1}, which is probably a consequence of the expansion of the radio plasma.

Furthermore, the material enveloping the radio jet is in a much higher ionization state than that of the surrounding NLR gas. The highest excitation is coincident with the jet axis, where emission in the coronal line of [Fe VII] λ3769 is detected and the He II λ4686 is strong but where [O II] λ3727 is depressed. This large localized increase in ionization on the jet axis is accompanied by the presence of an excess continuum. Because the electron density is substantially larger in the jet compared with the surrounding NLR, these results can be explained only if there is a more intense ionizing continuum associated with the jet. This can be accomplished in a variety of ways, which include an intrinsically anisotropic nuclear radiation field, a reduced gas covering factor, or the presence of a local ionization source.

The morphology, kinematics, and, possibly, the ionization structure of the NLR in the vicinity of the jet of NGC 1068 are a direct consequence of the interaction with the radio outflow.

Subject headings: galaxies: active — galaxies: individual (NGC 1068) — galaxies: Seyfert

1. INTRODUCTION

Extensive *Hubble Space Telescope* (*HST*) emission-line imagery of the narrow-line regions (NLRs) of Seyfert galaxies with linear radio sources has shown that the morphology of the NLRs is directly related to that of the radio emission. Seyfert galaxies with a lobelike radio morphology (e.g., Mrk 573, Mrk 78, NGC 3393, IRAS 0421+045, and IRAS 1105−035) have bow shock–shaped emission-line regions (Bower et al. 1994; Axon et al. 1989; Capetti et al. 1996), while those with a jetlike radio structure (e.g., Mrk 3, Mrk 348, Mrk 6, Mrk 1066) have jetlike emission-line structures (Bower et al. 1995; Capetti et al. 1995a, 1995b). These results have provided compelling evidence for strong dynamical interactions between the emission-line gas and radio-emitting ejecta on scales of ≤1 kpc.

The physical foundation of this picture was first developed by Taylor, Dyson, & Axon (1992), who constructed fast bow shock models for the interaction between radio ejecta and the ISM that included the effects of photoionization from the nucleus. Dopita & Sutherland (1996a, 1996b) have emphasized that the hot shocked gas could itself make an important local contribution to the ionizing continuum (becoming what they termed an *autoionizing* shock).

NGC 1068 is one of the closest Seyfert galaxies, and it harbors a bright radio source, with a prominent radio jet (Muxlow et al. 1996) terminating in an extended radio lobe (Wilson & Ulvestad 1983). Ground-based kinematic studies of the NLR have been carried out previously by a number of authors (Alloin et al. 1983; Baldwin et al. 1987; Meaburn & Pedlar 1986; Cecil, Bland, & Tully 1990; Unger et al. 1992; Arribas, Mediavilla, & Garcia-Lorenzo 1996) in [O III] λ5007. In particular, two broad components straddling a narrow central component in the northeast radio lobe were identified. The narrow component appears to follow the expected rotation curve of the galaxy and is emitted by undisturbed gas in the disk. At larger radii this triple structure disappears.

The complexity of the velocity field observed in the inner region is almost certainly due to the spatial confusion caused by projection and seeing effects, which mixes kinematic components from different regions along the line of sight. In particular, the velocity structure created by the expansion of the hot gas associated with the lobe is projected onto the region

[1] Based on observations with the NASA/ESA *Hubble Space Telescope*, obtained at the Space Telescope Science Institute, which is operated by AURA, Inc., under NASA contract NAS 5-26555 and by STScI grant GO-3594.01-91A.

[2] Affiliated to the Astrophysics Division, Space Science Department, ESA.

[3] On leave from the University of Manchester.

[4] Dipartimento di Astronomia e Scienza dello Spazio, Università di Firenze, Largo E. Fermi 5, I-50125, Italy.

[5] Osservatorio Astrofisico di Arcetri, Largo E. Fermi 5, I-50125, Italy.

interacting with the jet, which can be spatially resolved only with *HST*. In order to obtain a more detailed picture of the relationship between the velocity field and the ionization conditions in the NLR gas and the interaction of the gas with the radio jet, we have therefore obtained new long-slit spectroscopic observations with the Faint Object Camera (FOC) f/48 spectrograph on board the *HST*. Our results allow us to resolve the spatial confusion and provide evidence that shocks created by the jet play a key role in forming and, possibly, ionizing the NLR of NGC 1068. Throughout this Letter we will adopt a distance to NGC 1068 of 14.4 Mpc (Tully 1988), where 1″ corresponds to 72 pc.

2. OBSERVATIONS AND DATA REDUCTION

The NLR of NGC 1068 was observed using the FOC f/48 long-slit spectrograph on 1996 October 18 at resolutions of 1.78 Å and 0.″0287 pixel^{-1} along the dispersion and slit directions, respectively. The F305LP filter was used to isolate the first-order spectrum, which covers the 3650–5470 Å region and therefore includes the O II λ3727, Hβ λ4861, and O III λλ4959, 5007 emission lines. The slit, 0.″063 × 13.″5 in size, was placed at a position angle of 83° and spectra with exposure times of 627 s were taken in the 1024 × 512 nonzoomed mode at six locations separated by 1″. Unfortunately, owing to a guide star reacquisition failure, only three of the slit locations yielded usable spectra, which we identify as POS1, POS2, and POS3, respectively.

The data reduction follows the procedure described in detail by Macchetto et al. (1997). Flux calibration was performed using the observations of the spectrophotometric standard star LDS 749b.

To accurately determine the location of the slits, we compared the surface brightness profile derived from the FOC, f/96, F501N *HST* image of Macchetto et al. (1994) with that measured from the spectra at the three slit positions. The best match is displayed in Figure 1 (Plate L4) and is accurate to within half a slit width ($\simeq$0.″03).

The slit locations POS1 and POS2 cut across the emission-line filament system associated with the northern radio lobe (Capetti, Axon, & Macchetto 1997a), while the slit at POS3 (see Fig. 1) traverses cloud G (Evans et al. 1991) and the parallel feature to the west, which form a funnel-like structure where the jet meets the radio lobe (see Gallimore et al. 1996).

3. RESULTS

The velocities derived from the O III and O II lines by fitting Gaussian line profiles are plotted in Figure 2. Around the jet axis, at POS3 (Fig. 2*b*), the lines are split into two velocity systems separated by ~1500 km s^{-1}. Outside this region the gas motions are quiescent but with a gradient of +500 km s^{-1} from west to east. Notice that the velocity splitting is not symmetric about the systemic velocity but is much larger on the blueshifted side. The blueshifted component is also substantially brighter and has a larger velocity dispersion than the redshifted component. At POS2 (Fig. 2*a*) the velocity field is relatively flat, except at the filaments at slit coordinates ~−1″ to −2″, where there is a large redshifted velocity perturbation of amplitude ~300 km s^{-1}, at a similar radial velocity to that of the redshifted component of the split line region in POS3. POS1 (Fig. 2*a*) shows a similar pattern in velocity, but with a reduced amplitude in the perturbed region.

Turning to the emission-line strengths, in Figure 3 we show

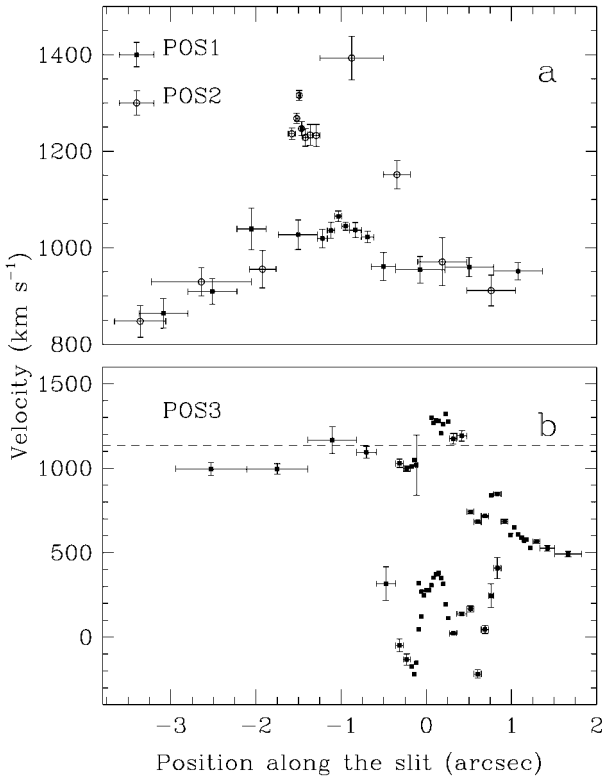

FIG. 2.—Velocity fields measured at the three slit positions. (*b*) Around the jet axis, at POS3, the gas is strongly kinematically perturbed and shows split lines with components separated by ~1500 km s^{-1}. The dashed lines mark the systemic velocity of NGC 1068 (Baan & Haschick 1983). (*a*) At POS2 and POS1 there are also large velocity perturbation at the location of the emission-line filaments.

plots of representative spectra from the five regions identified in Figure 1. On the jet axis (labeled as "Jet") the gas is highly ionized; Fe VII λ3759 and Ar IV are clearly visible and the He II λ4686 is as high as 0.7 times the strength of Hβ, while the O II emission appears to be depressed. This increase in excitation is accompanied by the presence of an excess local continuum, as shown in Figure 4 (Plate L5).

Outside the jet the excitation conditions are much lower, with O II being relatively stronger, particularly to the east, as shown in Figure 4. The variation of the O III/O II ratio along the slit, plotted in Figure 5, shows that there is a factor of $\simeq$5 difference between the ratio on the jet axis and outside. The electron temperature measured from the O III λλ4363/5007 ratio gives $T_e = (1.15 \pm 0.15) \times 10^4$ K. A lower limit for the electron density can be obtained from the Ar IV λλ4710/4740 ratio and yields $N_e \geq 10^{4.5}$ cm^{-3}. At similar distances from the nucleus, but off the jet, ground-based density measurements from the S II λλ6716/6731 ratio, obtained from our unpublished spectroscopy, indicate electron densities of a few 100 cm^{-3}. Thus, the increase in excitation on the jet occurs despite an increase in density.

4. DISCUSSION

The morphological connection between the optical and radio emission in the region of the jet has been discussed in detail by Gallimore et al. (1996) and by Capetti, Macchetto, & Lattanzi (1997b). They showed that there is a clear anticorrelation between radio and optical emission, with the brightest line-

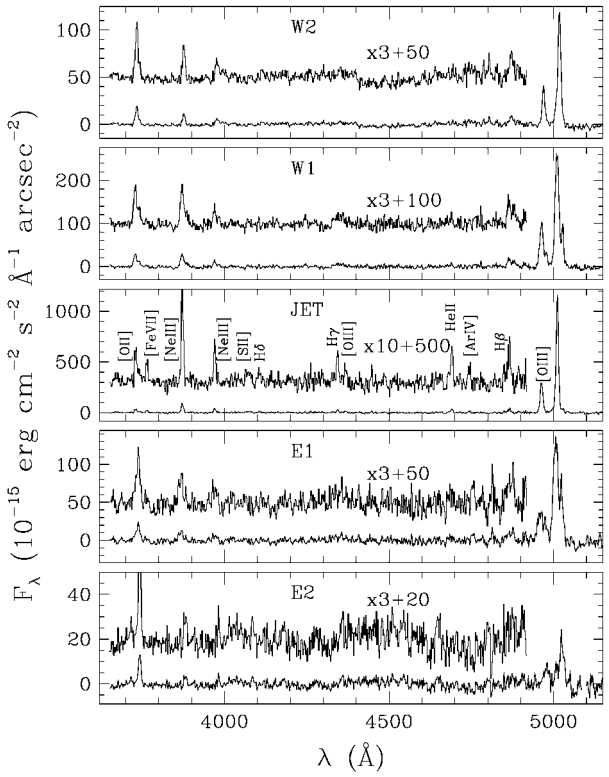

FIG. 3.—Spectra extracted at the positions indicated in Fig. 1. The spectrum extracted in a 0″.14 × 0″.063 aperture around cloud G, labeled "Jet," shows the high-excitation gas on the jet with Fe VII, Ar IV, and He II emission lines.

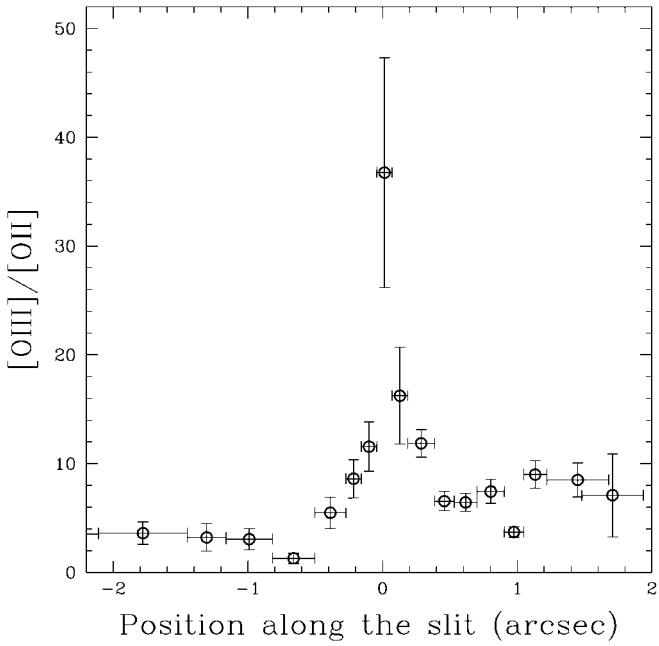

FIG. 5.—Plot of the O III/O II ratio as a function of position along the slit at POS3. The ratio reaches a maximum on the jet axis where it is ~5 times larger than that in the surrounding regions.

emitting knots surrounding the radio jet. In the jet-cloud interaction picture, the radio jet clears a channel through the cool ISM, leaving hot ionized gas in its wake and the line emission is highly enhanced along the edges of the radio jet where the gas is compressed.

The overall velocity structure and ionization conditions of the gas associated with the jet of NGC 1068 can be understood in terms of this picture of an expanding and cooling cocoon around the jet that creates very fast shocks with at least $V \simeq 700$ km s^{-1} (even when mass loading of the expanding cocoon is taken into account).

The viewing angle is such that to the NE the lobe is projected on to the disk of NGC 1068, so that the jet is seen emerging toward us out of the disk. The situation is very similar to that seen previously on the jet of 3C 120 (Axon et al. 1989), even down to the clumpy structure of the gas, which almost certainly arises because of the onset of instabilities caused by the mixing of hot and cold material. This morphology is again readily understood if it is due to the interaction between the jet and the surrounding medium. A viable explanation for the observed asymmetry of the velocity splitting is that it is due to density stratification of the disk; that is, the expanding hot bubble is able to expand more rapidly along the density gradient away from the disk plane than toward it. Further weight to this argument is provided by the systematic blueshift of coronal lines with respect to the lower excitation lines (Marconi et al. 1996). This implies that the coronal lines comes from a different kinematic component to which we would ascribe the hot cooling gas in the cocoon.

The spectral diagnostics obtained from our long-slit spectra indicate that the kinematically disturbed line-emitting gas associated with the radio jet has both a higher density and a higher excitation level than the surrounding NLR. A similar result, based on narrowband imaging, has been reported recently by Capetti et al. (1997a). The density enhancement is a factor of more than 100 if the ground-based measurements of the [S II] λλ6716/6731 ratio can be taken as typical of the regions extending away from the jet axis. On the other hand, the variations in the [O III] λ5007/[O II] λ3727 ratio along the POS3 slit imply a factor of 5 enhancement in the ionization parameter (U) across the jet axis (since this ratio is approximately proportional to U; Penston et al. 1990). The enhancements in both density *and* ionization parameter imply that the local ionizing radiation is a factor of ~500 higher at the location of the jet in POS3 than it is elsewhere. The exceptionally strong [Fe VII] and He II lines suggest that matter-bounded clouds might contribute significantly to the line emission near the jet. In this case, we will be overestimating the jump in U since low-ionization lines such as [O II] are strongly suppressed in such clouds. Nevertheless, this is unlikely to explain the whole of the inferred increase in the ionizing flux. Either a local ionization source is present that dominates the AGN radiation field near the jet axis, or the AGN radiation field is itself highly anisotropic.

The most important local ionization source is likely to be ionizing radiation (free-free and high-ionization line emission) from gas heated and ionized in fast shocks driven by the radio jet (Binette, Dopita, & Tuohy 1985; Sutherland, Bicknell, & Dopita 1993; Dopita & Sutherland 1996a, 1996b). The strong [Fe VII] emission and the excess continuum observed on the jet axis may be a clue that the coronal gas expected in this picture is indeed present. Alternatively, the on-axis increase in the ionizing flux could be attributed to intrinsic anisotropy of the nuclear continuum. In this case, the size of the enhancement in flux, and the fact that it is highly localized, requires a continuum beaming factor comparable with Doppler boosting in

a moderately relativistic jet (gamma a few). This idea can be ruled out because the region we have studied occurs after a significant bend of the jet and therefore one would expect to see higher excitation along the original jet direction, which is not observed (see Capetti et al. 1997a).

Perhaps a more likely explanation is that the continuum anisotropy is largely produced by azimuthal variations in the optical depth to ionizing photons. In this picture, the radio jet sweeps out a channel as it passes through the NLR with the result that ionizing radiation from the central source suffers much less attenuation along its axis than in other directions.

Our results on POS1 and POS2 can also be interpreted in terms of the interaction between the radio plasma and the ambient gas, but in this case it is the expanding lobe material that is driving the motion. From our spectroscopic data we can say little on the ionization conditions of these filaments because only the [O III] lines are detected.

5. CONCLUSIONS

We have presented new *HST* FOC f/48 long-slit spectra of the central 4″ of the NLR of NGC 1068. At a spatial scale of 0.″0287 pixel^{-1} these data provide an order-of-magnitude improvement in resolution over previous ground-based spectra and allow us to trace the interaction between the radio jet and the gas in the NLR. Our results show that, within $\pm 0.''5$ of the radio jet the emission lines are split into two components whose velocity separation is ~1500 km s^{-1} and are clearly the result of the interaction between the radio jet and the ambient NLR material. The filaments associated with the radio lobe also show a redshifted kinematic disturbance on the order of 300 km s^{-1}, which probably is a consequence of the expansion of the radio plasma.

Our results show that the highest excitation gas is physically related to the location of the jet and is accompanied by an excess continuum providing additional evidence for the interaction model.

The morphology, kinematics, and, possibly, the ionization structure of the NLR in the vicinity of the jet of NGC 1068 are a direct consequence of the interaction with the radio outflow.

A. M. acknowledges partial support through GO grant G005.44800 from Space Telescope Science Institute, which is operated by the Association of Universities for Research in Astronomy, Inc., under NASA contract NAS 5-26555. A. C. thanks the STScI visitor program for providing financial support during the course of this work. A. R. is supported by a Royal Society Fellowship. We thank E. Oliva for kindly providing his compilation of atomic parameters and his code to derive line emissivities.

REFERENCES

Alloin, D., Pelat, D., Boksenberg, A., & Sargent, W. 1983, ApJ, 275, 493
Arribas, S., Mediavilla, E., & Garcia-Lorenzo, B. 1996, ApJ, 463, 509
Axon, D. J., Capetti, A., Macchetto, F., Sparks, W. B., & Boksenberg, A. 1996, in Science with the *Hubble Space Telescope* II, ed P. Benvenuti, F. D. Macchetto, & E. J. Schreier (Baltimore: STScI), 214
Axon, D. J., Unger, S. W., Pedlar, A., Meurs, E. J. A., Whittle, D. M., & Ward, M. J. 1989, Nature, 341, 631
Baan, W. A., & Haschick, A. D. 1983, AJ, 88, 1088
Baldwin, J., Wilson, A. S., & Whittle, M. 1987, ApJ, 319, 84
Binette, L., Dopita, M. A., & Tuohy, I. R. 1985, ApJ, 297, 476
Bower, G., Wilson, A. S., Morse, J. A., Gelderman, R., Whittle, M., & Mulchaey, J. 1995, ApJ, 454, 106
Bower, G., Wilson, A. S., Mulchaey, J., Miley, G. K., Heckman, T. M., & Krolik, J. H. 1994, AJ, 107, 1686
Capetti, A., Axon, D. J., Kukula, M., Macchetto, F. D., Pedlar, A., Sparks, W. B., & Boksenberg, A. 1995a, ApJ, 454, 85
Capetti, A., Axon, D. J., & Macchetto, F. D. 1997a, ApJ, 487, 560
Capetti, A., Axon, D. J., Macchetto, F. D., Sparks, W. B., & Boksenberg, A. 1996, ApJ, 469, 554
Capetti, A., Macchetto, F. D., Axon, D. J., Sparks, W. B., & Boksenberg, A. 1995b, ApJ, 448, 600
———. 1995c, ApJ, 452, L87
Capetti, A., Macchetto, F. D., & Lattanzi, M. G. 1997b, ApJ, 476, 67
Cecil, G. B., Bland, J., & Tully, R. 1990, ApJ, 355, 70
Dopita, M. A., & Sutherland, R. S. 1996a, ApJ, 455, 468
———. 1996b, ApJS, 102, 161
Evans, I. N., Ford, H. C., Kinney, A. L., Antonucci, R. R. J., Armus, L., & Caganoff, S. 1991, ApJ, 369, 27
Gallimore, J. F., Baum, S. A., O'Dea, C. P., & Pedlar, A. 1996, ApJ, 458, 136
Macchetto, F. D., Capetti, A., Sparks, W. B., Axon, D. J., & Boksenberg, A. 1994, ApJ, 435, 15
Macchetto, F. D., Marconi, A., Axon, D. J., Capetti, A., Sparks, W. B., & Crane, P. 1997, ApJ, 489, 579
Marconi, A., van der Werf, P. P., Moorwood, A. F. M., & Oliva, E. 1996, A&A, 315, 335
Meaburn, J., & Pedlar, A. 1986, A&A, 159, 336
Muxlow, T. W. B., Pedlar, A., Holloway, A. J., Gallimore, J. F., & Antonucci, R. R. J. 1996, MNRAS, 278, 854
Penston, M. V., et al. 1990, A&A, 236, 53
Sutherland, R. S., Bicknell, G. V., & Dopita, M. A. 1993, ApJ, 414, 506
Taylor, D., Dyson, J., & Axon, D. J. 1992, MNRAS, 255, 35
Tully, R. B. 1988, Nearby Galaxies Catalog (Cambridge: Cambridge Univ. Press)
Unger, S. W., Lewis, J. R., Pedlar, A., & Axon, D. J. 1992, MNRAS, 258, 371
Wilson, A. S., & Ulvestad, J. S. 1983, ApJ, 275, 8

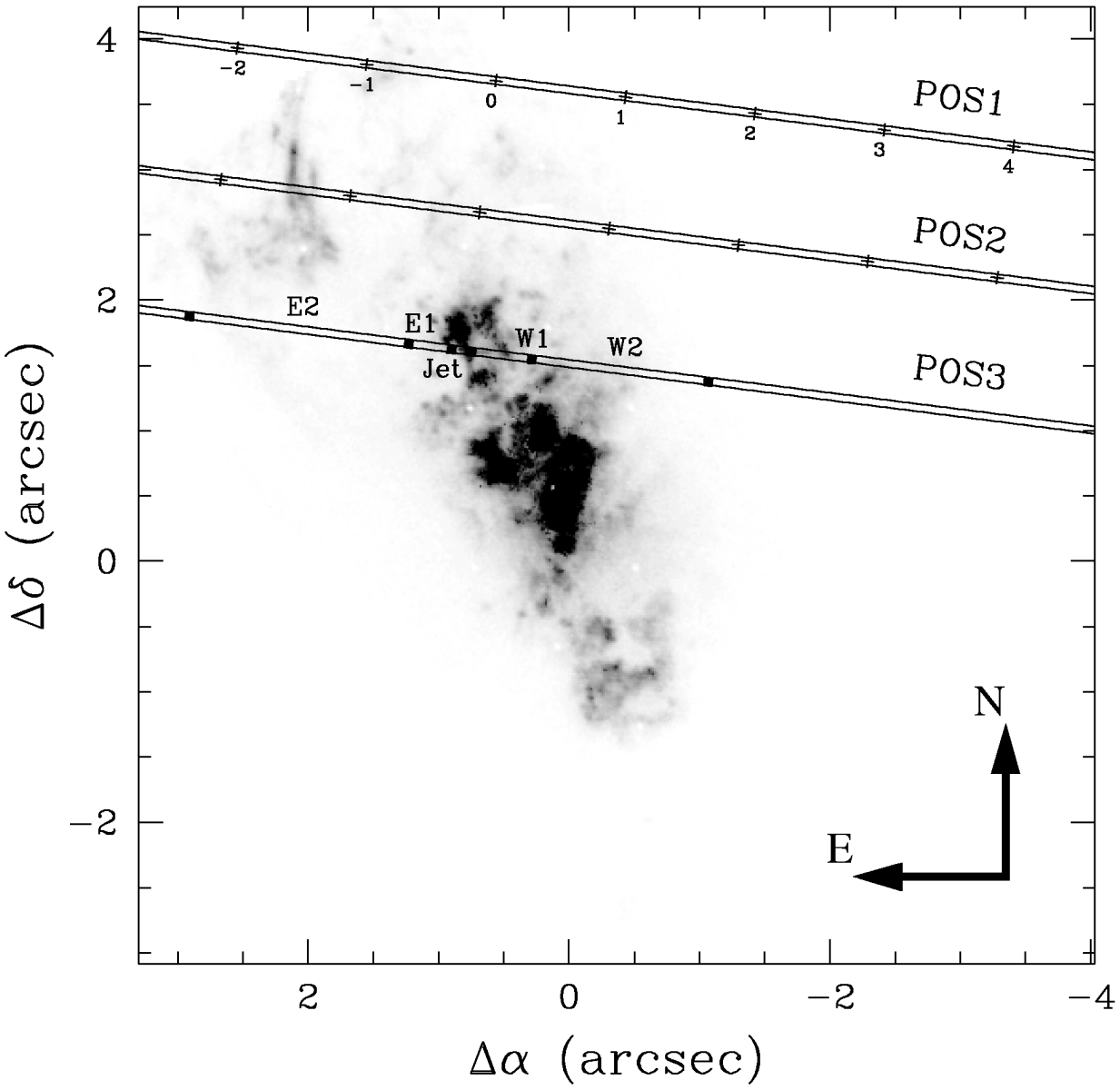

FIG. 1.—The slit positions used in our study overlaid on a gray-scale map of the O III image of Macchetto et al. (1994). The origin of the spatial axis on the borders of the image is centered on the position of the hidden nucleus (Capetti et al. 1995c). The spatial coordinates used along the slit are marked as crosses at POS1 and POS2. The zero point of this axis lies on cloud G in POS3. The filaments associated with the radio lobe intersect the slit at POS2 at location $-1''.5$ and POS1 at $-1''$. The filled squares at POS3 indicate the limits of the contiguous regions where we extracted the spectra shown in Fig. 3.

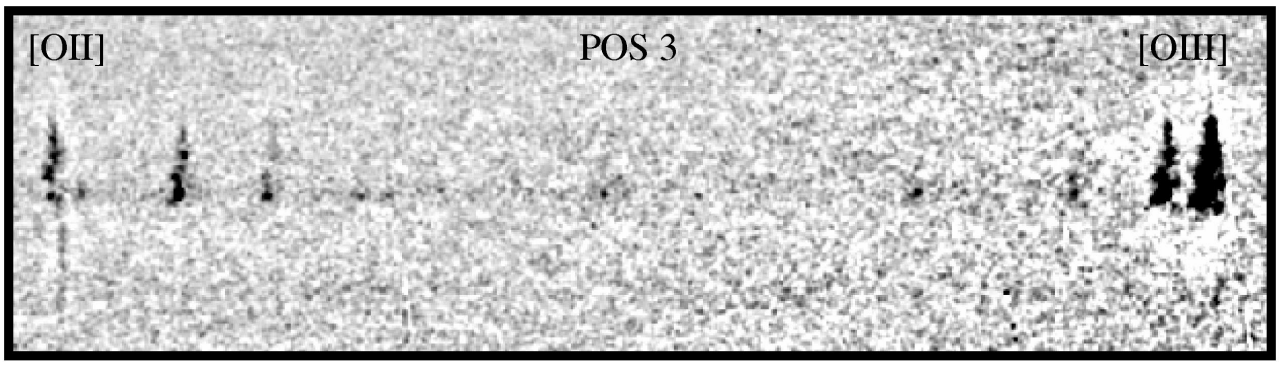

FIG. 4.—Gray-scale image of the spectrum at POS3 showing the excess continuum associated with the radio jet

AXON et al. (see 495, L76)